Thermal Spin Generator Based on a Germanene Nanoribbon Subjected to Local Noncollinear Exchange Fields

Jun Zheng*
College of New Energy, Bohai University, Jinzhou 121013, China
and Department of Physics and State Key Laboratory of Low-Dimensional Quantum Physics, Tsinghua University, Beijing 100084, China

Feng Chi
College of Engineering, Bohai University, Jinzhou 121013, China

Yong Guo†
Department of Physics and State Key Laboratory of Low-Dimensional Quantum Physics, Tsinghua University, Beijing 100084, China
and Collaborative Innovation Center of Quantum Matter, Beijing 100084, China

(Received 6 September 2017; revised manuscript received 13 December 2017; published 12 February 2018)

We theoretically propose a thermoelectric spin-current generator consisting of a zigzag germanene nanoribbon with thermal leads that are partially exposed to noncollinear exchange fields. Our results reveal that the exchange field in various regions and directions changes the helical edge states to different characteristics, and hence the pure spin current, the 100% spin-polarized current, and the pure charge current can be generated only under the temperature difference ΔT. The intertransformation between these three types of currents can be realized by tuning the relative angle of local exchange fields to $\theta = 0, 0.5\pi$, or π. It is worth noting that the pure spin current cannot be obtained without the temperature difference. We also find that the giant magnetoresistance can reach extremely large values in the bulk gap region by adjusting the exchange field of both leads to the x direction. All of the results indicate that the proposed germanene nanosystem is a promising candidate for spin caloritronic devices.

DOI: 10.1103/PhysRevApplied.9.024012

I. INTRODUCTION

Spintronics aims at exploiting the spin degrees of freedom to develop alternative generations of information storage and logic devices. Compared to charge-based conventional semiconductor devices, spintronic devices have many advantages, including increased integration densities and data processing and decreased electric power consumption [1]. The critical challenge of spintronics lies in how to generate, manipulate, and detect spin current. Alternative technologies have been adopted to manipulate the spin of an electron by, for instance, using magnetic materials and magnetic, electric, and optical fields [2].

With an increasing integration scale, heat dissipation becomes one of the major problems in high-density electronic devices and circuits. Conversion of waste heat into electricity is an essential topic for current and future technologies, including spintronics [3]. In view of potential applications in spintronic devices [4], there is currently great interest in the invigorated field of spin caloritronics, which focuses on the interplay of spin and heat currents [5]. Recently, Uchida *et al.* [6] and Slachter *et al.* [7] observed the spin Seebeck effect and the spin-dependent Seebeck effect, respectively, experimentally. These alternative thermoelectric phenomena offer an approach for controlling electron spin by utilizing the temperature, and they can be applied directly to thermoelectric spin generators [8]. Thermoelectric spin transport due to the spin Seebeck effect [9–16] and the spin-dependent Seebeck effect [17–24] has been widely studied in recent times.

Since the discovery of graphene, two-dimensional monolayer structures have attracted much interest in nanoscience and condensed-matter physics [25,26]. In the past few years, as an atomically thin layer of silicon (germanium), silicene [27–30] and germanene [31–34] have been synthesized on different substrate materials. Compared to graphene, silicene and germanene have more pronounced properties, such as the quantum spin Hall effect due to the spin-orbit interaction in the heavier atoms [35,36] and the buckled configurations from strong sp^3 bonding [37,38]. Because germanene has a larger band gap

*junzheng@semi.ac.cn
†guoy66@tsinghua.edu.cn

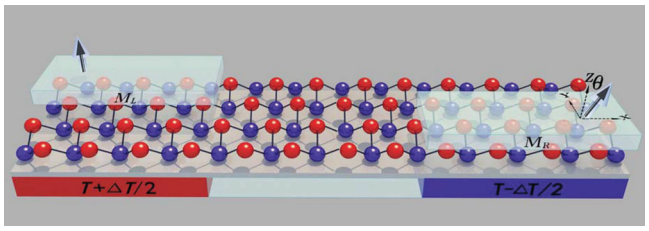

FIG. 1. Schematic of a germanene nanoribbon with partial noncollinear exchange fields. Orientations of the exchange field are indicated by the arrow, and θ is the angle between the exchange fields of the left and right leads. The temperatures of the leads are held at $T_L = T + \Delta T/2$ and $T_R = T - \Delta T/2$.

than silicene, the spin-related helical edge states of germanene are attractive candidates for high-temperature spintronic applications.

In this paper, we propose a thermal spin generator consisting of a germanene nanoribbon attached to two thermal leads that are subjected to local noncollinear exchange fields. As shown in Fig. 1, we apply the exchange fields to the upper half of the left germanene lead and the lower half of the right lead since the entire sample might not always be accessible due to the existence of a substrate, a gate, etc. In the following discussion, we focus on how the spin polarization of the current in the leads can reach either ∞, 100%, or 0, and how the giant magnetoresistance (GMR) can reach extremely large values just by adjusting the relative direction of the exchange fields.

II. MODEL AND METHODS

A generic buckled honeycomb germanene system can be described by the four-band tight-binding Hamiltonian $H = H_C + H_L + H_R$ [39–41], where

$$H_C = -t\sum_{\langle ij\rangle,\sigma} c^\dagger_{i\sigma}c_{j\sigma} + i\frac{\lambda_{\rm so}}{3\sqrt{3}}\sum_{\langle\langle ij\rangle\rangle,\sigma\bar{\sigma}} \nu_{ij}c^\dagger_{i\sigma}\sigma^z_{\sigma\bar{\sigma}}c_{j\bar{\sigma}} + \sum_{i,\sigma}\varepsilon_i c^\dagger_{i\sigma}c_{i\sigma},$$
$$H_L = H_C + M_L\sum_{i=1}^{N_y/2}\sum_{\sigma\bar{\sigma}} c^\dagger_{i\sigma}\sigma^{z(x)}_{\sigma\bar{\sigma}}c_{i\bar{\sigma}},$$
$$H_R = H_C + M_R\sum_{i=N_y/2+1}^{N_y}\sum_{\sigma\bar{\sigma}} c^\dagger_{i\sigma}\sigma^{\theta}_{\sigma\bar{\sigma}}c_{i\bar{\sigma}}. \quad (1)$$

Here, H_C, H_L, and H_R are the Hamiltonians of the central, left, and right germanene regions. i or j is the index of the discrete honeycomb lattice site, and $\langle ij\rangle$ ($\langle\langle ij\rangle\rangle$) run over all the nearest-neighbor (next-nearest-neighbor) hopping sites. The spin index $\sigma = \pm 1$ corresponds to spin-up ($\uparrow$) and spin-down ($\downarrow$) electrons. t is the nearest-neighbor hopping energy. The second term in H_C represents the effective spin-orbit coupling with strength $\lambda_{\rm so}$. $\nu_{ij} = \pm 1$ if the next-nearest hopping is counterclockwise (clockwise) around a hexagon with respect to the positive z axis. ε_i describes the on-site energy, and we set $\varepsilon_i = 0$ as the zero-energy point. The last terms in H_L and H_R represent the exchange fields applied in the upper half ($i \in [1, N_y/2]$) and lower half ($i \in [N_y/2+1, N_y]$) of the thermal leads with strength M_L and M_R. σ_z (σ_x) is the z (x) component of the Pauli matrix. $\sigma^\theta = \left[\begin{smallmatrix}\cos\theta & \sin\theta \\ \sin\theta & -\cos\theta\end{smallmatrix}\right]$, where θ is the relative angle between the left and right exchange fields. The direction of the exchange field can be tuned experimentally by applying an external field [42].

Using the Green's-function technique, the spin-dependent electric current in the α lead can be expressed in the Landauer formula form [43,44]:

$$J^\alpha_\sigma = \frac{e}{h}\int T_{e\sigma}[f_{L\sigma}(E) - f_{R\sigma}(E)]dE, \quad (2)$$

where $T_{e\sigma} = {\rm Tr}[\mathbf{\Gamma}_{L\sigma}\mathbf{G}^r_\sigma\mathbf{\Gamma}_{R\sigma}\mathbf{G}^a_\sigma]$ is the electronic transmission coefficient with the linewidth function $\mathbf{\Gamma}_{\alpha\sigma} = i(\mathbf{\Sigma}^r_{\alpha\sigma} - \mathbf{\Sigma}^a_{\alpha\sigma})$. The retarded Green's function is $\mathbf{G}^r_\sigma(E) = [\mathbf{G}^a_\sigma(E)]^\dagger = [E\mathbf{I} - \mathbf{H}_0 - \mathbf{\Sigma}^r_{L\sigma} - \mathbf{\Sigma}^r_{R\sigma}]^{-1}$, in which $\mathbf{H_0}$ is the Hamiltonian matrix of the central region and $\mathbf{\Sigma}^r_{\alpha\sigma}$ is the self-energy of the lead α. The retarded self-energy function can be obtained from $\mathbf{\Sigma}_{\alpha\sigma} = \mathbf{H}_{c\alpha}\mathbf{g}^r_{\alpha\sigma}\mathbf{H}_{\alpha c}$, where $\mathbf{H}_{c\alpha}$ is the coupling between the central region and the lead α value. The surface Green's function of semi-infinite germanene lead $\mathbf{g}^r_{\alpha\sigma}$ can be calculated using the transfer matrix [45], or the Green's-function method [46]. $f_\alpha(E) = [e^{(E-E_F)/k_BT_\alpha} + 1]^{-1}$ is the Fermi-distribution function with $T_{L(R)} = T \pm \Delta T/2$. Then, the spin and charge currents of the system are given by the formula $J_s = (J_\uparrow - J_\downarrow)$ and $J_c = (J_\uparrow + J_\downarrow)$ [47]. The spin polarization of the current under a thermal bias can be calculated using $P = (J_\uparrow - J_\downarrow)/(J_\uparrow + J_\downarrow)$.

III. RESULTS AND DISCUSSION

In our simulations, we choose the hopping energy t as the energy unit. In experiments, the reasonable hopping energy and effective spin-orbit coupling values for germanene are approximately 1.3 eV and 43 meV [35,48,49], and we fix $\lambda_{\rm so} = 0.03t$ throughout this paper. Figure 1 shows an exchange field uncovered area with $N_x = 9$ and $N_y = 4$. In all calculations, the width and length of the central region are chosen as $N_x = N_y = 80$, which is sufficiently large to avoid the finite-size effects on helical edge states [50]. By approaching the sample with ferromagnetic materials [51] or by doping with ferromagnetic dopants [52,53], the exchange field is successfully realized, and we let $M_L = M_R \simeq 5$ meV $= 0.003t$. The system equilibrium temperature and temperature difference are fixed at $T = 100$ K and $\Delta T = 10$ K, respectively. It should be noted that a larger temperature difference ΔT can be realized experimentally in a lateral structure if more unit cells are selected in the x direction.

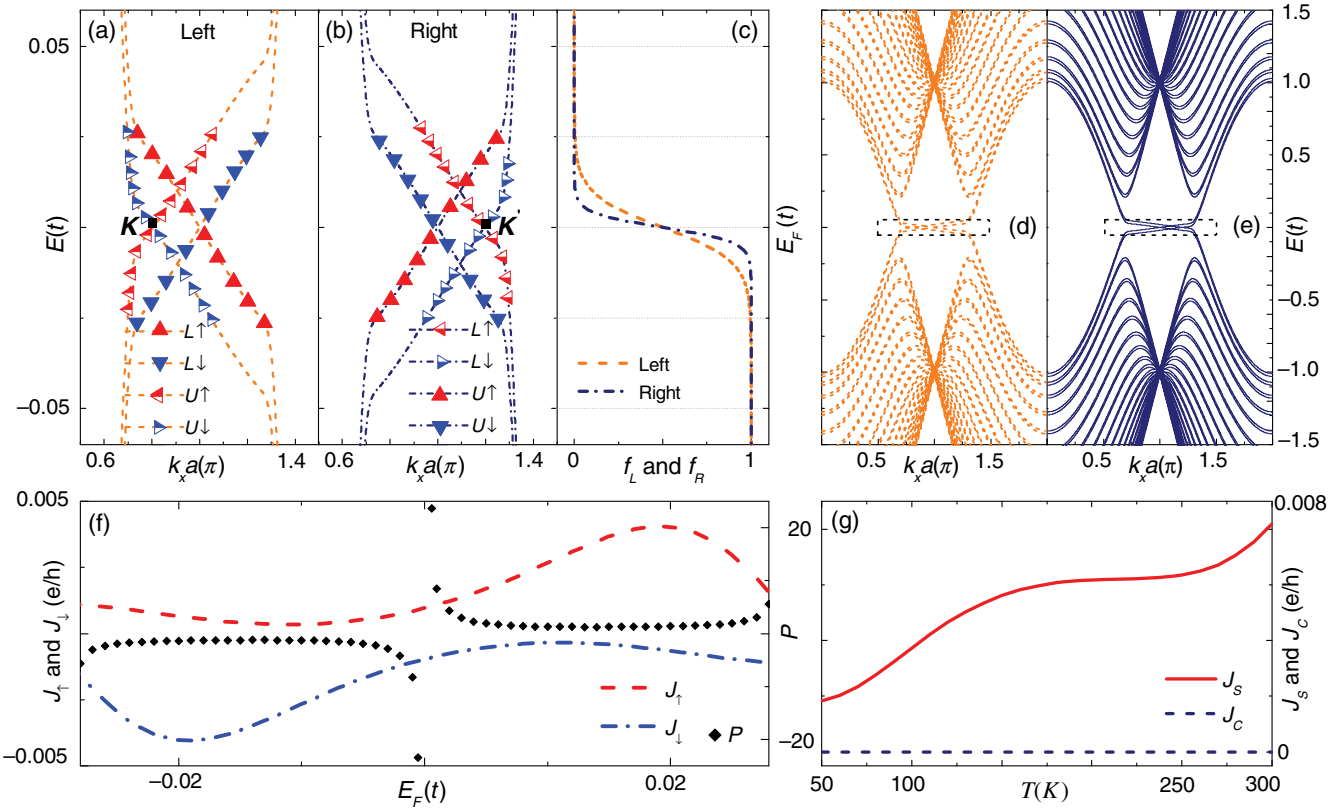

FIG. 2. (a) Edge states of the left germanene lead, the upper half of which is exposed to the z-direction exchange field. $L_{\uparrow(\downarrow)}$ corresponds to the spin-up (spin-down) lower-edge state and $U_{\uparrow(\downarrow)}$ is the upper-edge state transformed spin-up (spin-down) inner-edge state. (b) Edge states of the right germanene lead, the lower half of which is exposed to the z-direction exchange field. $L_{\uparrow(\downarrow)}$ corresponds to the lower-edge state transformed spin-up (spin-down) inner-edge state and $U_{\uparrow(\downarrow)}$ is the spin-up (spin-down) upper-edge state. (c) Fermi function of the thermal leads vs the Fermi energy E_F. Full band structures of the (d) left and (e) right germanene leads. (f) Spin-dependent current and spin polarization as a function of the Fermi energy E_F. (g) Spin and charge currents vs the system temperature with $E_F = 0$.

We first fix the exchange field on the upper half of the left lead along the z direction and consider the case of a noncollinear exchange field acting on the lower half of the right germanene leads, as shown in Fig. 1. For the case of $\theta = 0$ (parallel configuration), both the upper half of the left germanene lead and the lower half of the right lead are exposed to the out-of-plane z-direction exchange field. The band structures of the edge states are shown in Figs. 2(a) and 2(b), which correspond to the dotted rectangular shape of the full electronic spectrum in Figs. 2(d) and 2(e).

For the sake of contrast, before discussing the details of Figs. 2(a) and 2(b), let us remark that, without the external field ($M_L = M_R = 0$), the spin-up lower-edge state and the spin-down upper-edge state in the energy-band diagram of the leads are degenerate. Meanwhile, the spin-down lower-edge state is degenerate with the spin-up upper-edge state. The direction of motion is correlated with spin, the upper edge supports a forward mover with spin-up and a backward mover with spin-down, and conversely for the lower edge. The curves of these edge states (not shown) are exactly the same as $L_\uparrow$, $L_\downarrow$ in Fig. 2(a) and $U_\uparrow$, $U_\downarrow$ in Fig. 2(b). When applying the z-direction exchange field to the upper half of the left germanene lead (the lower half of the right lead), the time-reversal symmetry is broken, and the topological phase of the region with an external field is transformed into the trivial phase; as a result, the helical edge states at the upper (lower) edge are destroyed. As illustrated in Fig. 2(a) [Fig. 2(b)], states of different edges are nondegenerate and lead to inner states $U_\uparrow$ and $U_\downarrow$ ($L_\uparrow$ and $L_\downarrow$) intersecting at the K ($k_x a = \frac{4}{5}\pi$) [K' ($k_x a = \frac{6}{5}\pi$)] point. By contrast, one pair of states at the other edge (no exchange field applied) remains unaffected.

Owing to electrons of different spin in the helical edge states moving in opposite directions and the band-selective phenomenon [54], $j_\uparrow \neq j_\downarrow$, and the currents are spin polarized as shown in Fig. 2(f). It is interesting to point out that, with a temperature difference, there are more electrons (holes) being excited above (below) the Fermi energy in the hotter region [see Fig. 2(c)], and an equal number of spin-up electrons and spin-down holes could tunnel to the right lead when $E_F = 0$. Under this situation, the spin-up and -down currents are equal and opposite,

$J_\uparrow = -J_\downarrow$. The charge current $J_c = 0$; meanwhile, J_s still has a finite value. The spin polarization $P = (J_\uparrow - J_\downarrow)/(J_\uparrow + J_\downarrow)$ [see the diamond symbol and the right ordinate in Fig. 2(f)] can reach infinity, which means that a thermal bias induces only a pure spin current without charge current.

It should be emphasized that if there is only a voltage bias ΔV, it is impossible for electrons with different spin orientations to be transported in opposite directions. This is the case because, after expanding the Fermi-distribution function in Eq. (2) to the first order in temperature difference ΔT and voltage bias ΔV, the spin-resolved current can be expressed as $J_\sigma = G_\sigma \Delta V + G_\sigma S_\sigma \Delta T$, where $G_\sigma = e^2 \int dE(-\partial f/\partial E) T_{e\sigma}(E)/h$ is the spin-dependent conductance and $S_\sigma = \int dE(-\partial f/\partial E)(E - E_F) T_{e\sigma}(E)/[eT \int dE(-\partial f/\partial E) T_{e\sigma}(E)]$ is the spin-dependent Seebeck coefficient. If $\Delta T = 0$, the current is reduced to $J_\sigma = G_\sigma \Delta V$, in which the conductance G_σ is always greater than zero. $J_\sigma > 0$ or $J_\sigma < 0$ for a case in which $\Delta V > 0$ or $\Delta V < 0$; thus, $J_\uparrow$ and $J_\downarrow$ keep flowing in the same direction, and one could obtain a spin-polarized current ($J_s \neq 0$, $J_c \neq 0$) but not a pure spin current ($J_s \neq 0$, $J_c = 0$). However, a thermal bias makes it feasible to induce a pure spin current. When only the temperature difference exists (i.e., $\Delta T \neq 0$ and $\Delta V = 0$), it is easy to derive that $J_\sigma = G_\sigma S_\sigma \Delta T$, in which S_σ is an odd function of the Fermi energy E_F. Note that S_σ gains opposite contributions from electrons and holes and hence differs by sign for $E_F > 0$ and $E_F < 0$. Therefore, only under the temperature gradient could the flow pattern in Fig. 2(f) be obtained.

By increasing the system temperature, more electrons and holes can be excited and can participate in transport, but the symmetry between electrons and holes still holds with regard to $E_F = 0$. Therefore, as shown in Fig. 2(g), the pure spin current J_s increases rapidly with an increase in the system temperature T, while J_c remains zero. When $T = 300$ K and $\Delta T = 10$ K, the maximum pure spin current can reach approximately 0.4 μA and tends to increase with further enlargement of the temperature difference ΔT.

Turning the relative angle of exchange fields to $\theta = 0.5\pi$, the lower-half of the right lead is then exposed to the x-direction field. To clarify the transport properties of the carriers, we show the band structures of the right lead in Fig. 3(a). By applying the x-direction exchange field, the lower-half region changes into a topologically trivial phase, and the helical edge states located at the same edge disappear because of the breaking of local time-reversal symmetry and spin symmetry. Compared to the effect of the z-direction exchange field [see Fig. 2(b)], the inner-edge states do not emerge when the exchange field along the x axis is applied [see Fig. 3(a)]. Figure 3(b) shows the spin-resolved current J_σ and the spin polarization P as a function of the Fermi energy E_F. Within the bulk band gap, the

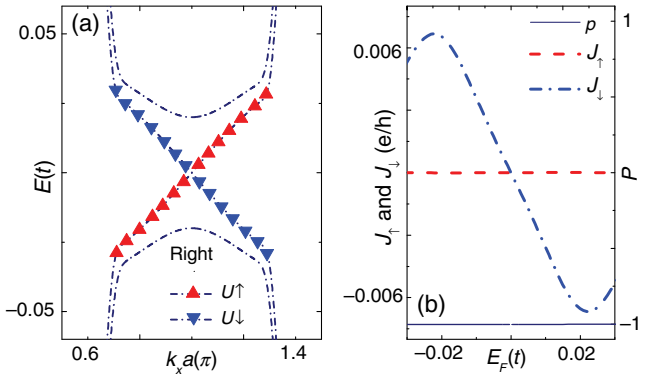

FIG. 3. (a) Edge states of the right germanene lead, the lower half of which is exposed to the x-direction exchange field. (b) Spin-dependent current and spin polarization as a function of the Fermi energy E_F.

values of the spin polarization under the solely thermal bias can be kept at a constant -1 [see the thin solid line in Fig. 3(b)]. Interchanging the exchange fields of the thermal leads, the spin polarization of electrons can reach $+1$ (omitted from Fig. 3 for the sake of clarity). This means that the germanene device can efficiently filter not only spin-up electrons but also spin-down electrons, over a broad range of energies. It is worth noting that the spin-filter effect can be observed only when the germanene nanoribbon is under the influence of the local exchange field.

For the relative angle of exchange fields $\theta = \pi$, the helical edge states at the lower edge are destroyed and lead to inner states at the K point owing to the $(-z)$-direction exchange field subjected to the right lead [see Fig. 4(a)]. In comparison to Fig. 2(b), in which the external field of the right lead is along the z direction, we note that the inner-edge states emerge around K point instead of around K'. Therefore, the band structure of the right lead is essentially the same as the left one. In Fig. 4(b), the electrons transported through the germanene nanoribbon are spin

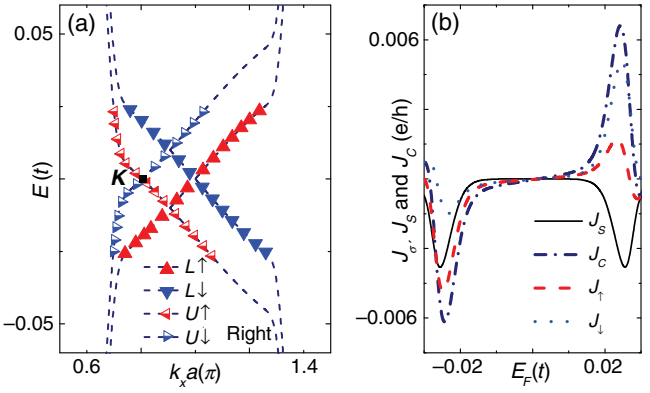

FIG. 4. (a) Edge states of the right germanene lead, the lower half of which is exposed to the $(-z)$-direction exchange field. (b) Spin-dependent current, spin, and charge currents as a function of the Fermi energy E_F.

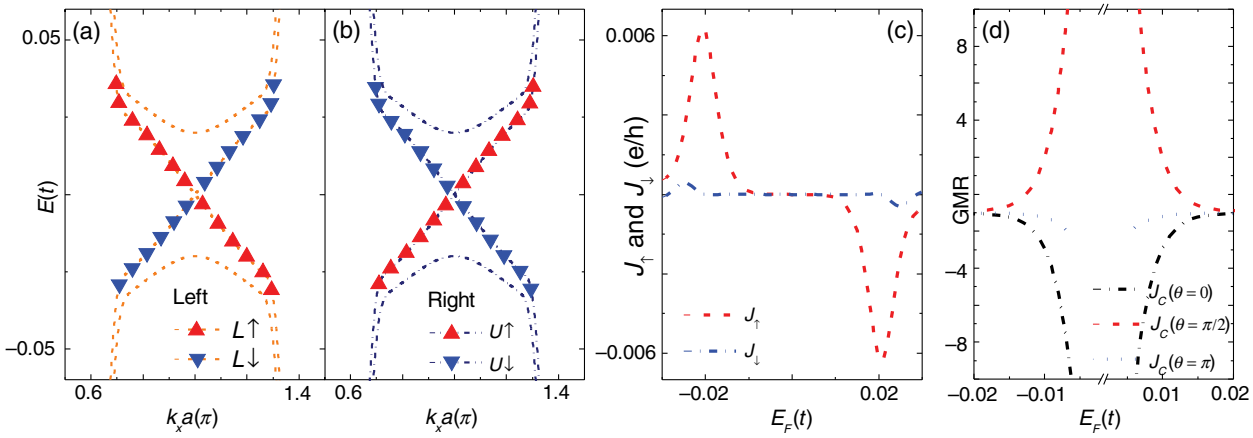

FIG. 5. Edge states of the (a) left and (b) right germanene leads with the x-direction exchange field. (c) Spin-dependent current and (d) giant magnetoresistance as a function of the Fermi energy E_F.

unpolarized, and the spin polarization $P=(J_\uparrow-J_\downarrow)/(J_\uparrow+J_\downarrow)$ is exactly zero, which means that a thermal gradient induces only a pure charge current without spin current.

Turning the thermal spin generator on or off by controlling the temperature of the leads is one of the most natural strategies. However, since germanene and silicene both have an extremely low thermal conductivity [55,56], a longer time is required to cancel the temperature difference ΔT, which results in a very low switching ratio. Here, we propose a more immediate way of turning off the spin generator, namely, by means of adjusting the exchange field of the left and right leads to the x direction. In this case, the upper-edge states of the left lead and lower-edge states of the right lead are broken, which are depicted in Figs. 5(a) and 5(b). The mismatch of edge modes makes both the spin and charge currents vanish within the bulk band gap [see Fig. 5(c)], and it can be used as a high-efficiency switch. The distinct orientations of the exchange field bring about completely different transport characteristics and give rise to the GMR effect, which can be described quantitatively by the ratio $\mathrm{GMR}=[I_c(\theta)-I_c(M_x)]/I_c(M_x)$, where $I_c(M_x)=I_\uparrow(M_x)+I_\downarrow(M_x)$ denotes the charge current flowing through the germanene system when the exchange field of the leads are along the x direction. The numerical results for the GMR corresponding to the current in Figs. 2(f) [$I_c(\theta=0)$], 3(b) [$I_c(\theta=\pi/2)$], and 4(b) [$I_c(\theta=\pi)$] are shown in Fig. 5(d). As demonstrated in Fig. 5(d), GMR may reach extremely large values when the Fermi energy E_F is around the band-gap center.

We now briefly discuss the effect of defect scattering on the spin-transport properties due to the fact that real materials always have nonmagnetic defects (such as edge roughness or structural defects) or magnetic defects (such as a magnetic domain boundary). Since nonmagnetic defect scattering does not break the time-reversal symmetry [57,58], the helical property of the edge states is topologically protected, and spin flips cannot be induced; therefore, all results in this paper can also be obtained in the presence of nonmagnetic defects.

IV. CONCLUSIONS

In summary, we theoretically investigate in this paper thermoelectric spin transport through a germanene nanoribbon, where the left and right germanene thermal leads are subjected to exchange fields at different locations. It is found that the thermoelectric spin properties can be strongly modulated by the orientation of exchange fields. When the exchange fields of both leads are perpendicular to the plane ($\theta=0$), the pure spin current can be generated only if a temperature difference exists. In addition, J_s values increase rapidly upon enhancing the system temperature and temperature gradient. For the $\theta=0.5\pi$ case (i.e., when the exchange field of the right lead lies in the plane), the germanene device can efficiently filter not only spin-up electrons but also spin-down electrons over a broad range of energies. When the exchange field at one lead is antiparallel to that of the other lead ($\theta=\pi$), the temperature difference induces only a pure charge current without a spin current. We also find that, by adjusting the exchange field of the leads to the x direction, the GMR emerges; meanwhile, the spin-current generator can be rapidly and effectively turned off.

ACKNOWLEDGMENTS

This work was supported by the National Natural Science Foundation of China (Grants No. 11604021, No. 11547209, and No. 11574173), the Doctoral Scientific Research Foundation of Liao Ning Province (Grant No. 201601352), and the Open Project of State Key Laboratory of Low-Dimensional Quantum Physics (Grant No. KF201613).

[1] S. A. Wolf, D. D. Awschalom, R. A. Buhrman, J. M. Daughton, S. V. Molnar, M. L. Roukes, A. Y. Chtchelkanova, and D. M. Treger, Spintronics: A spin-based electronics vision for the future, Science **294**, 1488 (2001).

[2] I. Zutic, J. Fabian, and S. D. Sarma, Spintronics: Fundamentals and applications, Rev. Mod. Phys. **76**, 323 (2004).

[3] Y. Dubi and M. D. Ventra, Colloquium: Heat flow and thermoelectricity in atomic and molecular junctions, Rev. Mod. Phys. **83**, 131 (2011).

[4] A. Hoffmann and S. D. Bader, Opportunities at the Frontiers of Spintronics, Phys. Rev. Applied **4**, 047001 (2015).

[5] G. E. W. Bauer, E. Saitoh, and B. J. V. Wees, Spin caloritronics, Nat. Mater. **11**, 391 (2012).

[6] K. Uchida, S. Takahashi, K. Harii, J. Ieda, W. Koshibae, K. Ando, S. Maekawa, and E. Saitoh, Observation of the spin Seebeck effect, Nature (London) **455**, 778 (2008).

[7] A. Slachter, F. L. Bakker, J. P. Adam, and B. J. V. Wees, Thermally driven spin injection from a ferromagnet into a nonmagnetic metal, Nat. Phys. **6**, 879 (2010).

[8] H. Adachi, K. Uchida, E. Saitoh, and S. Maekawa, Theory of the spin Seebeck effect, Rep. Prog. Phys. **76**, 036501 (2013).

[9] C. M. Jaworski, J. Yang, S. Mack, D. D. Awschalom, J. P. Heremans, and R. C. Myers, Observation of the spin Seebeck effect in a ferromagnetic semiconductor, Nat. Mater. **9**, 898 (2010).

[10] S. Y. Huang, W. G. Wang, S. F. Lee, J. Kwo, and C. L. Chien, Intrinsic Spin-Dependent Thermal Transport, Phys. Rev. Lett. **107**, 216604 (2011).

[11] P. H. Chang, F. Mahfouzi, N. Nagaosa, and B. K. Nikolic, Spin Seebeck effect on the surface of a topological insulator due to nonequilibrium spin polarization parallel to the direction of thermally driven electronic transport, Phys. Rev. B **89**, 195418 (2014).

[12] M. Wierzbicki, J. Barnas, and R. Swirkowicz, Thermoelectric properties of silicene in the topological and band insulator states, Phys. Rev. B **91**, 165417 (2015).

[13] H. H. Fu, D. D. Wu, L. Gu, M. H. Wu, and R. Q. Wu, Design for a spin-Seebeck diode based on two-dimensional materials, Phys. Rev. B **92**, 045418 (2015).

[14] I. Diniz and A. T. Costa, Microscopic origin of subthermal magnons and the spin Seebeck effect, New J. Phys. **18**, 052002 (2016).

[15] J. D. Arboleda, O. A. Olmos, M. H. Aguirre, R. Ramos, A. Anadon, and M. R. Ibarra, Spin Seebeck effect in a weak ferromagnet, Appl. Phys. Lett. **108**, 232401 (2016).

[16] N. Okuma, M. R. Masir, and A. H. Macdonald, Theory of the spin-Seebeck effect at a topological-insulator/ferromagnetic-insulator interface, Phys. Rev. B **95**, 165418 (2017).

[17] J. C. L. Breton, S. Sharma, H. Saito, S. Yuasa, and R. Jansen, Thermal spin current from a ferromagnet to silicon by Seebeck spin tunnelling, Nature (London) **475**, 82 (2011).

[18] Z. P. Niu and S. H. Dong, Valley and spin thermoelectric transport in ferromagnetic silicene junctions, Appl. Phys. Lett. **104**, 202401 (2014).

[19] A. Torres, M. P. Lima, A. Fazzio, and A. J. R. da Silva, Spin caloritronics in graphene with Mn, Appl. Phys. Lett. **104**, 072412 (2014).

[20] Y. S. Liu, X. Zhang, J. F. Feng, and X. F. Wang, Spin-resolved Fano resonances induced large spin Seebeck effects in graphene-carbon-chain junctions, Appl. Phys. Lett. **104**, 242412 (2014).

[21] B. Z. Rameshti and A. G. Moghaddam, Spin-dependent Seebeck effect and spin caloritronics in magnetic graphene, Phys. Rev. B **91**, 155407 (2015).

[22] X. Yang, J. Zheng, F. Chi, and Y. Guo, Spin power and efficiency in an Aharnov-Bohm ring with an embedded magnetic impurity quantum dot, Appl. Phys. Lett. **106**, 193107 (2015).

[23] J. Zheng, F. Chi, and Y. Guo, Exchange and electric fields enhanced spin thermoelectric performance of germanene nanoribbon, J. Phys. Condens. Matter **27**, 295302 (2015).

[24] S. Kolenda, M. J. Wolf, and D. Beckmann, Observation of Thermoelectric Currents in High-Field Superconductor-Ferromagnet Tunnel Junctions, Phys. Rev. Lett. **116**, 097001 (2016).

[25] A. H. C. Neto, F. Guinea, N. M. R. Peres, K. S. Novoselov, and A. K. Geim, The electronic properties of graphene, Rev. Mod. Phys. **81**, 109 (2009).

[26] A. K. Geim and K. S. Novoselov, The rise of graphene, Nat. Mater. **6**, 183 (2007).

[27] P. Vogt, P. De Padova, C. Quaresima, J. Avila, E. Frantzeskakis, M. C. Asensio, A. Resta, B. Ealet, and G. Le Lay, Silicene: Compelling Experimental Evidence for Graphenelike Two-Dimensional Silicon, Phys. Rev. Lett. **108**, 155501 (2012).

[28] A. Fleurence, R. Friedlein, T. Ozaki, H. Kawai, Y. Wang, and Y. Y. Takamura, Experimental Evidence for Epitaxial Silicene on Diboride Thin Films, Phys. Rev. Lett. **108**, 245501 (2012).

[29] L. Meng, Y. L. Wang, L. Z. Zhang, S. X. Du, R. T. Wu, L. F. Li, Y. Zhang, G. Li, H. T. Zhou, W. A. Hofer, and H. J. Gao, Buckled silicene formation on Ir (111), Nano Lett. **13**, 685 (2013).

[30] D. Chiappe, E. Scalise, E. Cinquanta, C. Grazianetti, B. van den Broek, M. Fanciulli, M. Houssa, and A. Molle, Two dimensional Si nanosheets with local hexagonal structure on a MoS_2 surface, Adv. Mater. **26**, 2096 (2014).

[31] L. F. Li, S. Z. Lu, J. B. Pan, Z. H. Qin, Y. Q. Wang, Y. L. Wang, G. Y. Cao, S. X. Du, and H. Gao, Buckled germanene formation on Pt(111), Adv. Mater. **26**, 4820 (2014).

[32] M. E. Davila, L. Xian, S. Cahangirov, A. Rubio, and G. Le Lay, Germanene: A novel two-dimensional germanium allotrope akin to graphene and silicene, New J. Phys. **16**, 095002 (2014).

[33] M. Derivaz, D. Dentel, R. Stephan, M. C. Hanf, A. Mehdaoui, P. Sonnet, and C. Pirri, Continuous germanene layer on Al(111), Nano Lett. **15**, 2510 (2015).

[34] L. Zhang, P. Bampoulis, A. N. Rudenko, Q. Yao, A. V. Houselt, B. Poelsema, M. I. Katsnelson, and H. J. W. Zandvliet, Structural and Electronic Properties of Germanene on MoS_2, Phys. Rev. Lett. **116**, 256804 (2016).

[35] C. C. Liu, W. X. Feng, and Y. G. Yao, Quantum Spin Hall Effect in Silicene and Two-Dimensional Germanium, Phys. Rev. Lett. **107**, 076802 (2011).

[36] L. Seixas, J. E. Padilha, and A. Fazzio, Quantum spin Hall effect on germanene nanorod embedded in completely hydrogenated germanene, Phys. Rev. B **89**, 195403 (2014).

[37] K. Takeda and K. Shiraishi, Theoretical possibility of stage corrugation in Si and Ge analogs of graphite, Phys. Rev. B **50**, 14916 (1994).

[38] S. Cahangirov, M. Topsakal, E. Akturk, H. Sahin, and S. Ciraci, Two- and One-Dimensional Honeycomb Structures of Silicon and Germanium, Phys. Rev. Lett. **102**, 236804 (2009).

[39] C. L. Kane and E. J. Mele, Z_2 Topological Order and the Quantum Spin Hall Effect, Phys. Rev. Lett. **95**, 146802 (2005).

[40] M. Ezawa, A topological insulator and helical zero mode in silicene under an inhomogeneous electric field, New J. Phys. **14**, 033003 (2012).

[41] X. T. An, Y. Y. Zhang, J. J. Liu, and S. S. Li, Spin-polarized current induced by a local exchange field in a silicene nanoribbon, New J. Phys. **14**, 083039 (2012).

[42] A. Mougin, T. Mewes, M. Jung, D. Engel, A. Ehresmann, H. Schmoranzer, J. Fassbender, and B. Hillebrands, Local manipulation and reversal of the exchange bias field by ion irradiation in FeNi/FeMn double layers, Phys. Rev. B **63**, 060409 (2001).

[43] Y. Meir and N. S. Wingreen, Landauer Formula for the Current Through an Interacting Electron Region, Phys. Rev. Lett. **68**, 2512 (1992).

[44] A. P. Jauho, N. S. Wingreen, and Y. Meir, Time-dependent transport in interacting and noninteracting resonant-tunneling systems, Phys. Rev. B **50**, 5528 (1994).

[45] D. H. Lee and J. D. Joannopoulos, Simple scheme for surface-band calculations. I, Phys. Rev. B **23**, 4988 (1981).

[46] D. H. Lee and J. D. Joannopoulos, Simple scheme for surface-band calculations. II. The Green's function, Phys. Rev. B **23**, 4997 (1981).

[47] Q. F. Sun, H. Guo, and J. Wang, A Spin Cell for Spin Current, Phys. Rev. Lett. **90**, 258301 (2003).

[48] W. A. Harrison, *Electronic Structure and the Properties of Solids* (Dover, New York, 1989).

[49] M. Ezawa, Spin valleytronics in silicene: Quantum spin Hall–quantum anomalous Hall insulators and single-valley semimetals, Phys. Rev. B **87**, 155415 (2013).

[50] B. Zhou, H. Z. Lu, R. L. Chu, S. Q. Shen, and Q. Niu, Finite Size Effects on Helical Edge States in a Quantum Spin-Hall System, Phys. Rev. Lett. **101**, 246807 (2008).

[51] P. Wei, F. Katmis, B. A. Assaf, H. Steinberg, P. J. Herrero, D. Heiman, and J. S. Moodera, Exchange-Coupling-Induced Symmetry Breaking in Topological Insulators, Phys. Rev. Lett. **110**, 186807 (2013).

[52] R. Yu, W. Zhang, H. J. Zhang, S. C. Zhang, X. Dai, and Z. Fang, Quantized anomalous Hall effect in magnetic topological insulators, Science **329**, 61 (2010).

[53] Y. L. Chen, J. H. Chu, J. G. Analytis, Z. K. Liu, K. Igarashi, H. H. Kuo, X. L. Qi, S. K. Mo, R. G. Moore, D. H. Lu, M. Hashimoto, T. Sasagawa, S. C. Zhang, I. R. Fisher, Z. Hussain, and Z. X. Shen, Massive Dirac fermion on the surface of a magnetically doped topological insulator, Science **329**, 659 (2010).

[54] J. Nakabayashi, D. Yamamoto, and S. Kurihara, Band-Selective Filter in a Zigzag Graphene Nanoribbon, Phys. Rev. Lett. **102**, 066803 (2009).

[55] S. Balendhran, S. Walia, H. Nili, S. Sriram, and M. Bhaskaran, Elemental analogues of graphene: Silicene, germanene, stanene, and phosphorene, Small **11**, 640 (2015).

[56] X. L. Zhang, H. Xie, M. Hu, H. Bao, S. Yue, G. Z. Qin, and G. Su, Thermal conductivity of silicene calculated using an optimized Stillinger-Weber potential, Phys. Rev. B **89**, 054310 (2014).

[57] M. Z. Hasan and C. L. Kane, Colloquium: Topological insulators, Rev. Mod. Phys. **82**, 3045 (2010).

[58] X. L. Qi and S. C. Zhang, Topological insulators and superconductors, Rev. Mod. Phys. **83**, 1057 (2011).